ANALYSIS OF CRC PAVEMENT UNDER MOISTURE, TEMPERATURE, AND CREEP EFFECTS

Subrahmanya M. Kadiyala
Design Engineer
Dreco Inc.

Dan G. Zollinger
Assistant Professor
Texas A&M University

ABSTRACT

A numerical procedure is presented for studying the effects of steel reinforcement and environmental parameters on the early-aged behavior of continuously reinforced concrete (CRC) pavements. The numerical procedure consists of two stages. The first stage predicts shrinkage strains developed due to moisture loss in the concrete pavement. It uses the semi-discrete method of nonlinear finite element analysis to predict the moisture distribution in CRC pavement as a function of time. This model is verified with published theoretical and experimental results. An existing finite element model (originally developed for the analysis of moisture distribution in subgrade materials) is modified and adapted for moisture distribution analysis in concrete pavements.

Both shrinkage and thermal strains are determined in two stages of analysis. Shrinkage strains (predicted in the first stage) and the thermal strains (predicted in second stage) imposed due to variations in ambient temperature are used as input to the stress analysis. The second stage predicts stress distribution taking into account concrete creep in the pavement after initial development of the crack pattern. The CRC pavement is represented in the finite element analysis with two-dimensional plane strain elements. Bond slip is modeled at the interface of concrete and steel. Analysis of the internal restraint is performed to determine subsequent concrete pavement stresses due to environmental effects. A finite element code was developed specifically for the prediction of the resultant stresses in the concrete pavement.

INTRODUCTION

Continuously reinforced concrete (CRC) pavements are constructed with closely spaced, parallel rows of steel reinforcement placed in an uninterrupted, longitudinal configuration. Consequently, the pavement contains reinforcement (in approximately 18 meter lengths) placed continuously end for end for long distances with no transverse expansion joints. Hence, from a structural point of view, this type of pavement consists of an infinite continuum in one direction (i.e., longitudinal direction). However, due to the combination of environmental and wheel loads, a characteristic crack pattern develops that consists of a distribution of transverse cracks. Initial cracking in CRC pavements is largely affected by environmentally induced temperature and moisture gradients which cause slab curling. Field observations of initial cracks suggest that these cracks form within the first few days after placement of the concrete. Subsequent cracks form due to the continuity of reinforcement (i.e., internal restraint) which inhibits free movement of the concrete matrix after the formation of initial cracks. Stresses that are developed at this stage are referred to

as restraint stresses.

Various factors affecting the formation of cracks in CRC pavements at an early age of concrete are considered in this study. CRC pavement typically is allowed to develop a random crack pattern that is primarily governed by various environmental conditions at the time of construction, mix design factors, curing practice, etc. These cracks are also governed by other material factors, such as tensile strength of concrete and the type of coarse aggregate. Transverse crack intervals vary from 0.5 to 4 meters, but sometimes may occur within 15 centimeter intervals, which is undesirable. Most of the transverse cracks form shortly after construction of the slab and sometimes may not be evident on the surface for a period of time. Recent field studies (16) have comfirmed this conclusion. The final crack pattern (as observed on the pavement surface) typically stabilizes approximately three years after construction however, 80 to 90 percent of the crack pattern typically develops between 28 to 90 days after construction.

The objective of this work is to develop a numerical framework to study the various factors affecting the crack formation in early aged CRC pavement based on two-dimensional analysis (in terms of slab thickness and longitudinal dimension). The word framework is used since the focus of this effort is to identify and include models to address the development of transverse cracking in CRC pavement, to formulate a working analysis process with these models, and to illustrate some typical results from the analysis. The ambient climatic conditions and structural configuration of CRC pavement are the primary causes for the development of tensile stresses in the pavement. Of the different numerical models developed for this analysis, one of them pertains to the computation of shrinkage strains due to decrease in moisture content of pavement and another one pertains to the stresses due to the combination of shrinkage and thermally-related strains. The thermal strains are the result of a decrease in the temperature of the concrete which may occur under seasonal climatic changes.

BEHAVIORAL CHARACTERISTICS OF CRC PAVEMENTS

Design analysis of CRC pavements is based on the determination of stresses and strains in the steel and concrete caused by restraint of environmentally induced volumetric changes and those of wheel loads. This restraint also develops a characteristic crack pattern which influences the strength of the pavement. Hence, the prediction of crack spacing is also an integral part of the design process. Vetter (1) developed relationships for crack spacing, in reinforced concrete, along with bond stress and tensile stress with respect to the restrained shrinkage and thermal strains. Some of the assumptions made in the development of these relationships are the following:

1) Stresses due to restraint of volumetric

strains are uniformly distributed over the pavement section; i.e., plane sections remain plane within the concrete pavement.

2) Midway between the cracks, the change in length of the reinforcing steel and the concrete are equal which means that strain compatibility exists in the bonded regions of the reinforcement. In these regions, there is no relative movement between the concrete and the steel reinforcement, and therefore, no bond stresses or changes in stress in the concrete or the steel occur.

3) The total bond force developed between the reinforcement and the concrete is equal to either the total tensile force in the concrete or the total change in the force in the steel. The force in the steel reinforcement is transferred from the steel to the concrete by the bond stress acting along the bar.

Other models (developed by Friberg (2), McCullough et al. (3), Palmer et al. (14)) for the prediction of crack spacing, made improvements over Vetter's model, in characterizing bond slip relationsships. However all these models fail to consider the variation of shrinkage strains, through thickness of the pavement. The consideration of uniform shrinkage with respect to the depth of the pavement may be a reasonable approximation for matured concrete, but a highly inappropriate approximation for early-aged concrete. The consideration of moisture and temperature gradients in the concrete pavement will also allow for important effects of consideration of curling and warping stresses in the analysis. A procedure is developed to compute moisture content at different depths of concrete based on diffusion theory developed by Bazant (4).

In the approach taken for consideration of moisture gradients in the slab, the finite element procedure is used for spatial approximation and the finite difference procedure for time approximation. The finite element method, used in this manner, has an added advantage of adaptability to any geometry with ease when compared to the finite difference method. Many empirical models are available in literature to predict temperatures at different depths of a concrete pavement as a function of the ambient temperature at the pavement site.

A typical segment of CRC pavement is illustrated in Figure 1 in the first few days after construction of pavement. It is observed that the cracks are parallel to each other and transverse in direction. Figure 2 represents the assumptions used by Vetter to account for the longitudinal reinforcement on a per unit area of pavement cross-section. Therefore, short pavement segments can be modeled for further analysis by approximating the slab as a three-layered system based on plane strain assumptions. The middle layer is a composite layer consisting of steel and concrete connected by bond slip elements.

The rate of variation of material properties is very high prior to the concrete achieving complete maturity (i.e., before 28

days). Since this work was mainly focused onthe stress state and behavior of concrete in the first 7 days of pavement life, consideration of this variability is important for this study.

Gardner and Poon (5) discussed time and temperature effects on various concrete properties and also their affect on the bond relationship. Experimental investigation was performed to study these factors. Laboratory

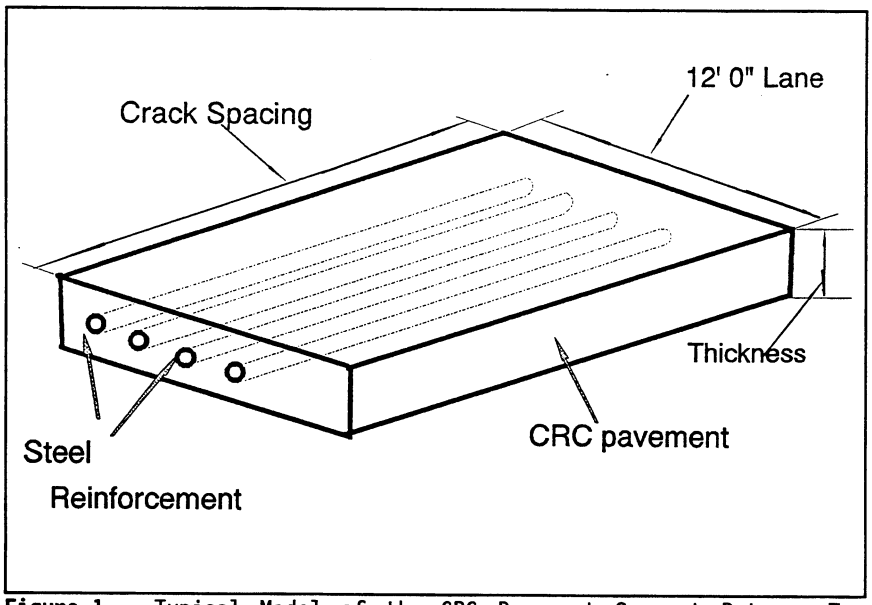


Figure 1. Typical Model of the CRC Pavement Segment Between Two Adjacent Cracks.

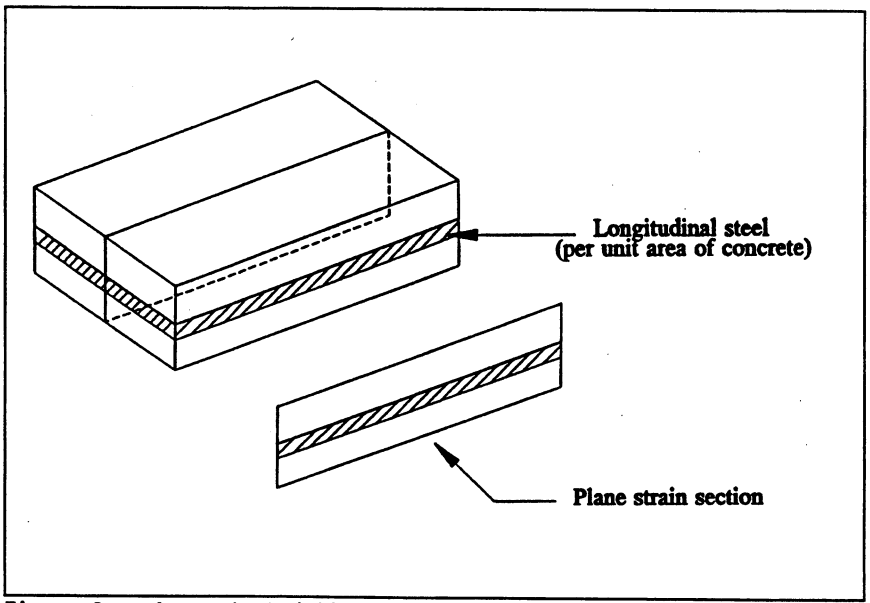


Figure 2. Approximated Three Layered View of the Pavement and the Cross-Section Considered for Plane Strain Analysis.

molds were prepared in which compression, tensile and bond strength tests were performed. It was found that temperature influences tensile strength in much the same manner that it affects the compressive and bond strengths. Bond strength and tensile strength are observed to be proportional to the power 0.8 of the cylinder strength at the appropriate age.

ANALYSIS FRAMEWORK

Temperature drop and drying shrinkage causes volumetric change in the cracked pavement which may develop further cracking due to the restraint provided by the steel reinforcement. If the pavement is free to move, then it does not experience any stress (be it tensile or compressive), but if it is fully or partially restrained then stresses are developed in the concrete as illustrated in Figures 3 and 4 (17). If the tensile stress in a given layer exceeds the tensile strength of concrete, then the concrete cracks. Typically, the strength of early aged concrete is low and since the diffusion of moisture may be very high during this period, shrinkage strains can be dominant factors in the development of initial cracking and even in subsequent cracking. The following mathematical models were developed for estimating the shrinkage strains for the prediction of stresses leading to subsequent cracking. Their effect is combined with that of thermal strains to predict a final stress state in CRC pavement.

Drying Shrinkage Model

The prediction of drying shrinkage is based upon the following model suggested by Bazant and Najjar (4):

$$\nabla(k_h \nabla(h)) + \frac{\partial h_h}{\partial t} + K\frac{\partial T}{\partial t} = \frac{\partial h}{\partial t} \qquad [1]$$

where

k_h	=	diffusivity of concrete
h	=	percentage moisture content of the concrete at a given time
h_h	=	percentage moisture content due to hydration
T	=	temperature at different points in the concrete and at time intervals
K	=	hygrometric coefficient
t	=	time

The 'K' coefficient in equation 1 is a conversion coefficient which converts temperature differentials into an equivalent change of relative humidity. An approximate equation for 'K' that is dependent on 'h' can be given as (4):

$$K = 0.0135h\frac{(1-h)}{(1.25-h)} \quad \text{per } °C \qquad [2]$$

Equation 2 is an empirical approximation based on theoretical and experimental data. No flow boundary conditions are used on all surfaces for equation 1 for plane problems which are described by the following equation:

$$k_h\frac{\partial h}{\partial x}n_x + k_h\frac{\partial h}{\partial y}n_y = 0.0 \qquad [3]$$

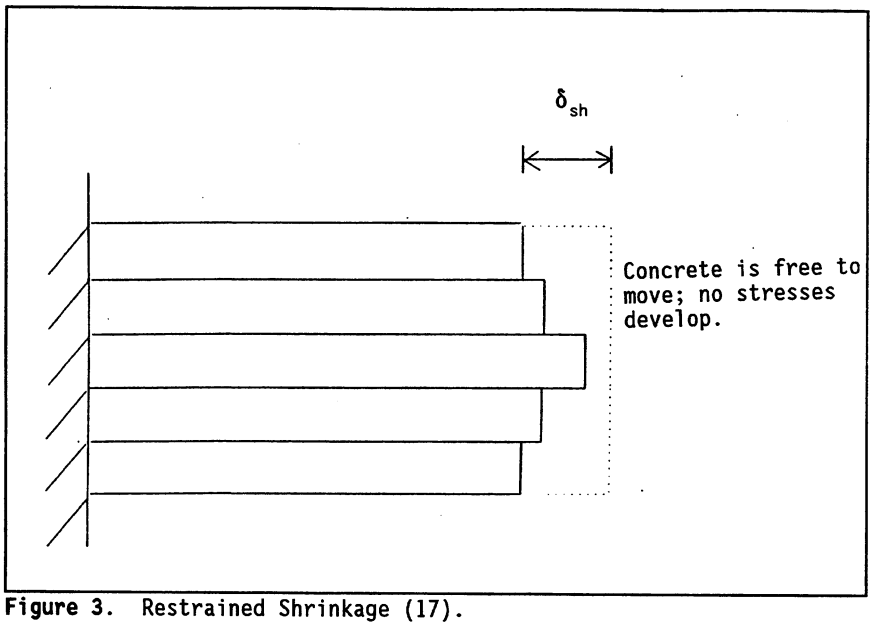


Figure 3. Restrained Shrinkage (17).

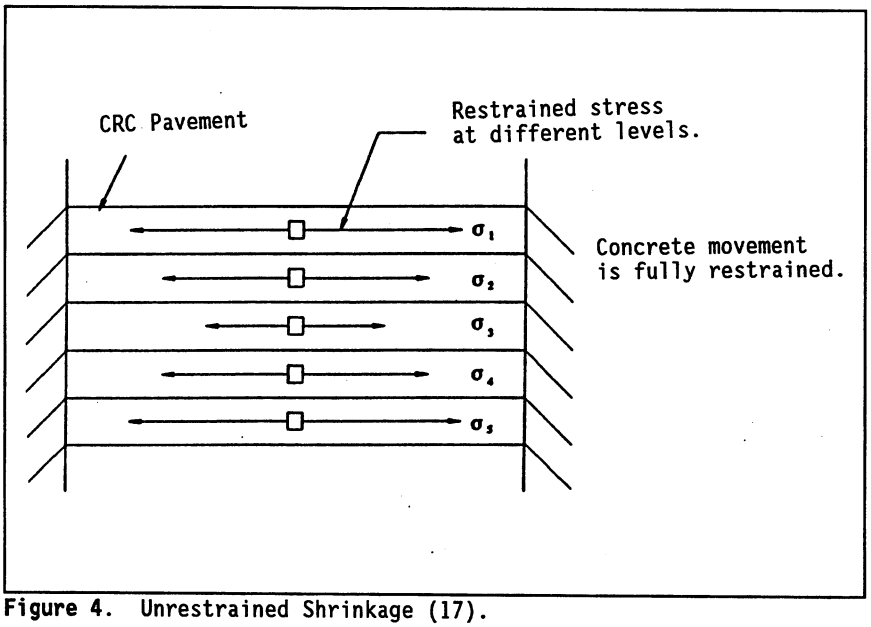


Figure 4. Unrestrained Shrinkage (17).

where n_x and n_y are direction cosines in x and y directions. The following are the imposed environmental humidity at the surface of the pavement:

$$h=\hat{h} \quad \text{on } \Gamma_2 \quad t\geq 0 \qquad [4]$$

where

Γ_2 = boundary surface where environmental humidity acts

h = moisture content on surface (environmental humidity)

It is assumed at the initial condition of time 't' = 0 that h_o = 100% (i.e., concrete is assumed to be completely

saturated). The k_h term in equation 1 is determined by the following equation (4):

$$(k_h)_t = k_d\left[\alpha_0+\frac{1-\alpha_0}{1+\left[\frac{1-H_t}{1-H_c}\right]^n}\right] \qquad [5]$$

where

k_d = diffusivity of concrete at h = 1 and a given temperature (cm^2/day)
α_0 = min k_h / max k_h (a constant for a given concrete mix)
n = a constant which characterizes the distribution of h about k_h
H_c = humidity value which corresponds to the average value of k_h
H_t = humidity value at the given time step 't'

Values of diffusivities of concrete are typically high for early aged concrete which rapidly decreases over the first seven days as the concrete matures. Diffusivity values (k_d) used later in an example analysis are taken from labortory experiments performed at Texas A&M University (Han, *unpublished data*) using psychrometers embedded in hardening concrete which provided data over several days monitoring the variations in moisture due to imposed wetting and drying cycles. The variations in the measurements of this nature are, at a minimum, subject to the affects of the material parmeters represented by the terms in equation 5. Equation 5 provides an estimate of the expected value of K_h as it varies with time. Variability in K_h will be encompassed within the variations of α_0, n, and H_c which may be defined in terms of any number of variance methods available in the literature which is not considered any further in this study. However, the material parameter n varies between 6 and 16 (4) and is found from the 'best fit' of computed diffusivity data to measured relative humidity data for a given mix.

The above nonlinear differential equation represents a classical boundary value problem. Bazant and Najjar (4) and also Grzybowski (6) solved this equation using a finite difference method. For generalized boundary conditions and geometries, the finite element method (FEM) is more convenient to use. In this study, the analysis is facilitated using the finite element method and is similar to the analysis of transient heat transfer. The solution is obtained using a semi-discrete approximation (i.e., spatial approximation is considered first, followed by an approximation in time). The differential equation is solved by an iterative procedure which converges to within a given tolerance. Temperature differentials and differentials of moisture loss due to hydration (or self-desiccation) are specified as input. Moisture loss from the concrete pavement is converted into shrinkage strains at any vertical position in the slab using the following equation for plain concrete (18):

$$\epsilon_{sh} = \epsilon_{sh\infty}(1-h^3) \qquad [6]$$

where h is previously defined, and the ultimate concrete shrinkage ($\epsilon_{sh\infty}$), which is a material parameter of plain concrete. The following empirical expression (19) is used to compute $\epsilon_{sh\infty}$:

$$\epsilon_{sh\infty} = 1330-970y \qquad [7]$$

where

$$y = (390z^{-4}+1)^{-1} \qquad [8]$$

and equation 9:

$$z = 0.381\sqrt{f_{cyl28}}\left[1.25\sqrt{\frac{a}{c}} + 0.5\left(\frac{g}{c}\right)^2\right]\sqrt[3]{\frac{1+\frac{s}{c}}{\frac{w}{c}}} - 12$$

where

a/c = total aggregate/cement ratio
g/c = coarse aggregate/cement ratio
s/c = fine aggregate/cement ratio
w/c = water/cement ratio

Equation 6 is assumed to be applicable to the analysis of shrinkage strain in CRC pavement since previous studies have sucessfully applied the above expressions to concrete specimens in pure tension (6). Development and validation of equation 7 is documented elsewhere (19).

Figure 5 gives a typical finite element mesh used in this shrinkage analysis. The analysis performed is unidirectional, and hence only one column of elements through the slab (Figure 5) is used for the specific cases considered in this analysis. The assumption of one-dimensional drying idealizes the drying conditions in actual concrete pavements. However, it is noted that if the subbase layer is stabilized with asphaltic cement or similar material, a certan amount of impermeability exists at the interface between the bottom of the concrete pavement and the top of the subbase. This assumption would not be applicable to all types of subbases. Shrinkage strains of this model are used as input for the stress model applied to CRC pavement.

The Stress Model

Finite element (FE) stress analysis was performed for imposed strains in early aged concrete. The increase of strength and elasticity of concrete with age is accounted for in the analysis. Typically, the increase in strength of concrete at an early age (i.e., within the first few days) is very high. The variation of modulus of elasticity and strength of concrete is given by following empirical equations (6):

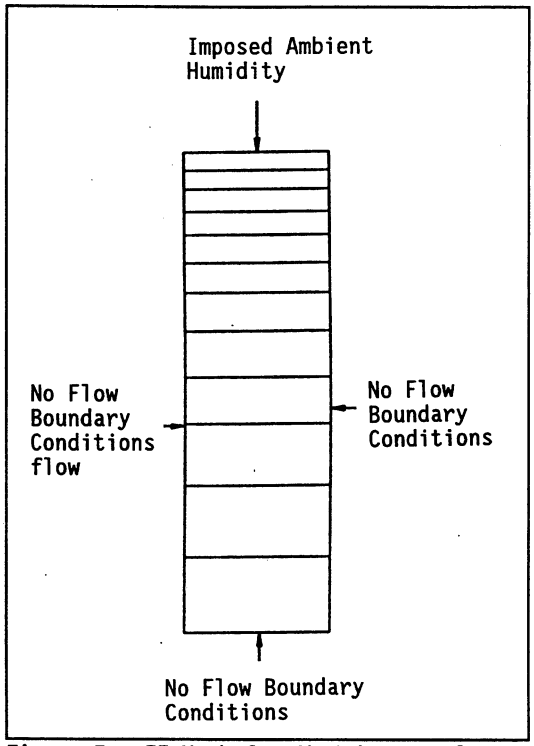


Figure 5. FE Mesh for Shrinkage Analysis.

$$f_c(t) = \frac{t}{A+Bt} f_c(28) \qquad [10]$$

$$E_c(t) = E_c(28)\sqrt{\frac{t}{A+Bt}} \qquad [11]$$

where

t = time (days)

$f_c(t)$ = compressive or tensile strength of concrete at time 't' (MPa)
$f_c(28)$ = compressive or tensile strength of concrete after 28 days (MPa)
$E_c(t)$ = modulus of elasticity at time t (MPa)
$E_c(28)$ = modulus of elasticity after 28 days (MPa)
A & B = constants depending on concrete mix (A = 4.00 and B = 0.85 for moist cured concrete, cement type I)

Characteristics of early-aged cracking behavior of CRC pavement may be illustrated in Figures 6a and 6b which summarizes the range in cracking data (both minimum and maximum crack intervals) collected from a recently constructed CRC pavement section near Houston, Texas. It is interesting to note that the initial cracking development occurs quickly (say over a three to five day period) once cracking begins to develop. The effect of moisture and temperature gradients on early-age cracking may be reflected in the combination of frictional, curing, and warping stresses. The curling and warping stress are typically characterized in terms of the radius of relative stiffness (ℓ). The range of ℓ - values for concrete pavements may vary between 90 to 110 centimeters. Bradbury (7) pointed out that long slabs (sections of concrete pavements with joint or crack spacing (L) greater than or equal to 12ℓ), as in the case of newly placed concrete pavements (whether jointed or CRC), develop maximum curling or warping stresses at a distance of 4.44ℓ from the joint or transverse crack. This effect, which is generally known and accepted from field experience, is manifest in actual pavements by cracks (whether random or controlled) occurring on the average at the interval pointed out above. Therefore, one would expect that stresses when combined with those due to frictional effects will contribute to cracking, at an early age, in CRC pavement at least at an interval of 4.44ℓ. The stresses that occur due to the restraint caused by the reinforcement may be accounted for at intervals less than this, since the stresses at intervals greater than L/ℓ of 4.44 are largely influenced by curling affects. Other factors also affect the rate of crack development such as coarse aggregate type (as shown in Figures 6a and 6b) and season or time of construction. It appears that an interval of L/ℓ equal to 4.44 or less may be appropriate to begin analyisis of restraint cracking due to reinforcement and frictional affects. In the example analysis discussed later, it is assumed that the pavement develops primary cracks at a spacing of eight feet as influenced by slab curling and warping which is approximately equal to 50 percent of 4.4ℓ.

Plane strain conditions are assumed for the stress analysis and the properties of steel and concrete in the model are considered to be independent of each other. Bond slip elements are incorporated at the interface between concrete and steel. Analysis is performed to predict secondary crack formation. The method suggested by Ngo and Scordelis (8) is considered for modeling the concrete in which the concrete

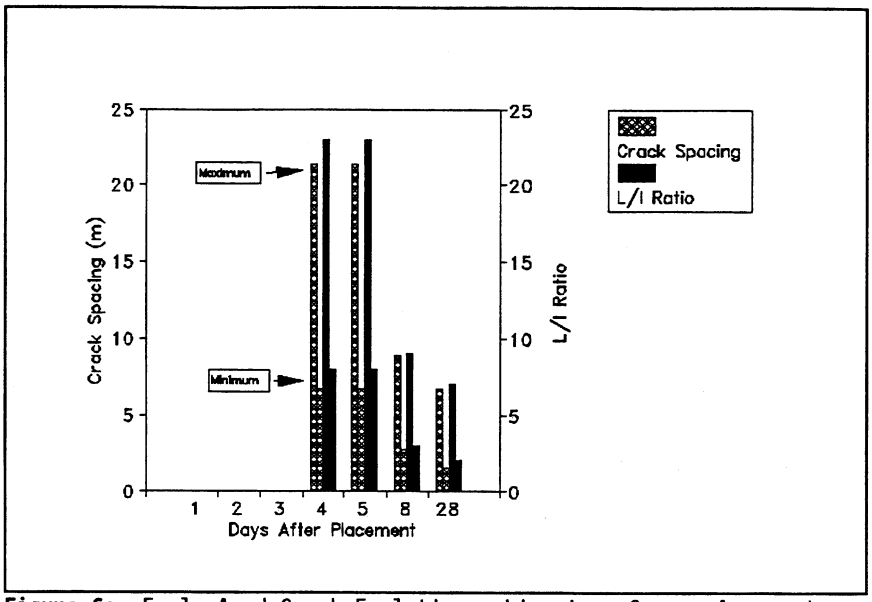


Figure 6a. Early-Aged Crack Evolution - Limestone Coarse Aggregate.

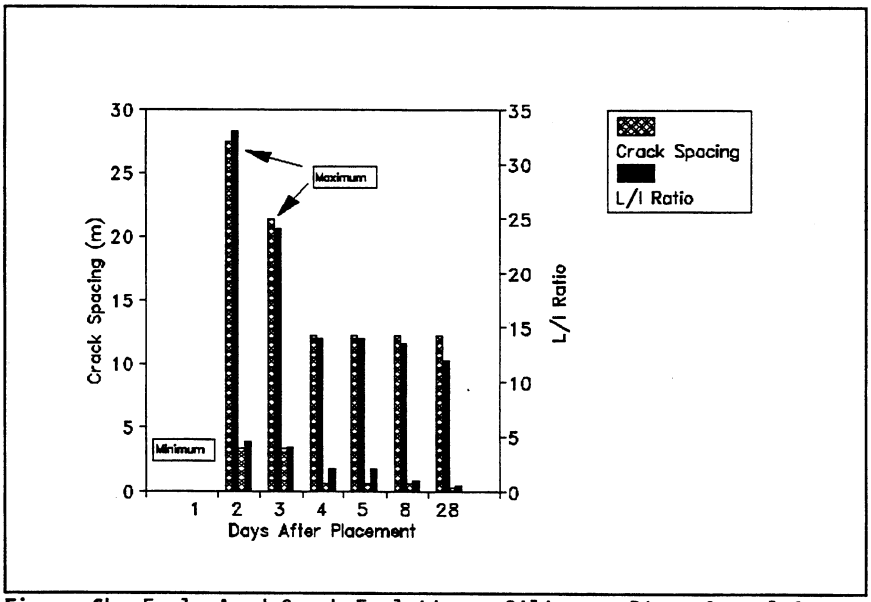


Figure 6b. Early-Aged Crack Evolution - Siliceous River Gravel Coarse Aggregate.

and steel are partitioned into two segments at the level of reinforcement. The thickness of these segments depends upon the percentage of steel reinforcement in concrete. This approach is shown in Figure 7. Eight-noded isoparametric elements with 3 x 3 Gaussian quadrature are used in the finite element analysis for both the concrete and the reinforcing steel. Strains are imposed by means of nodal forces. Stress transfer between steel and concrete due to bond is modeled using a bond slip element. A slip element has two degrees of freedom per node or four degrees of freedom per element at the interface of concrete and steel elements. It is assumed that x and y displacements of the spring

element are independent of each other. The element is as shown in Figure 8. Large values are given for the stiffness of the spring in the normal direction, so that the ratio of displacements in the normal direction to that of the reinforcing steel are approximately zero. The level of stiffness (depending modulus of elasticity of the concrete and surface characteristics of the steel bar) is assigned as input to the stiffness in the direction aligned with the steel is dependant upon the bond-slip relationship at the steel-concrete interface. The bond-slip function (as pointed out above) may vary depending on the bar pattern and the concrete properties. The spring stiffness is nonlinear and is approximated by the curve shown in Figure 9 (u = bond stress and δ = bond slip) which consists of two straight lines which is considered accurate enough to model the effect of bond-slip into the stress analysis. This is an approximation of the relationship suggested by Nilson (9) and recently validated by Jiang et al (21). Since the reinforcing steel is placed, in most instances, near the nuetral axis, plate bending has nominal affect on the resultant bond stress and therefore is normally not considered. This is particularily applicable where in CRC pavement segments the L/ℓ ratio is typically much less than 5.0 which is the threshold level to fully develop an interior load condition (23).

Model Boundary Conditions

Boundary conditions are shown in Figure 10. Symmetry is considered and only one-half of the crack spacing is analyzed for stresses. The line of symmetry is modeled as pin connected. It is assumed that the pavement subbase is rigid and that the bond between the pavement and subbase is negligible. Consequently, due to negligible friction on the analysis, the pavement is supported on rollers at its base. This assumption appears to be appropriate because it has been noted (10,22) that in the analysis of the structural respones for CRC pavements the effect of subbase friction is negligible for secondary cracking. However, the approach to the characterization of bond-slip at the steel concrete interface may also be applied to the friction between the concrete pavement and the subbase layer (14).

The stress-free boundary of concrete segment under consideration is taken as the crack face which is assumed to have developed after the first few days, as explained previously due to pavement curling stress. It is also assumed that formation of the crack releases all restraint along that boundary in the concrete. The steel is fixed on both sides since it is continuous across the crack face and theoretically continues infinitely in a CRC pavement. Thus, steel restraint of the longitudinal direction causes stresses in the steel and concrete and affects the bond stress between concrete and steel.

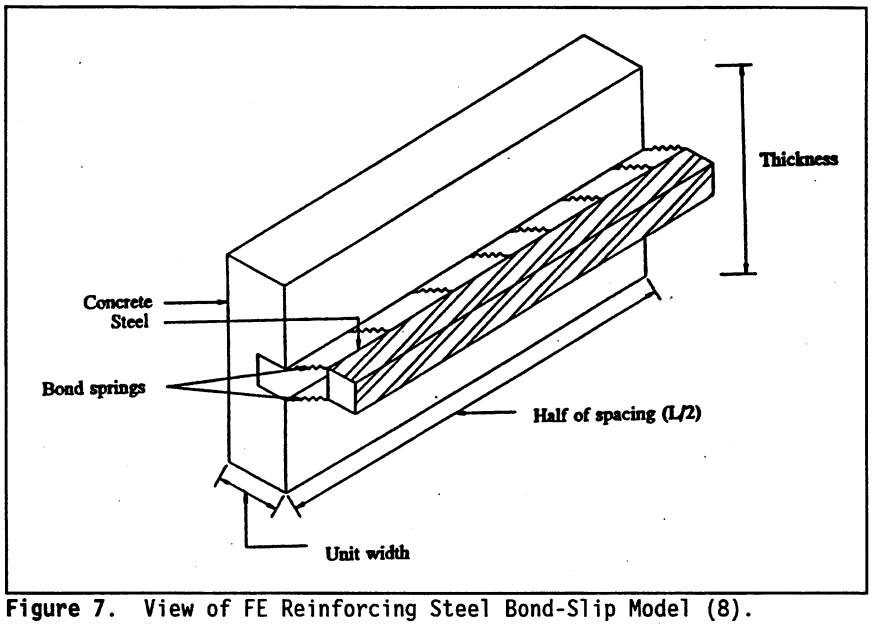


Figure 7. View of FE Reinforcing Steel Bond-Slip Model (8).

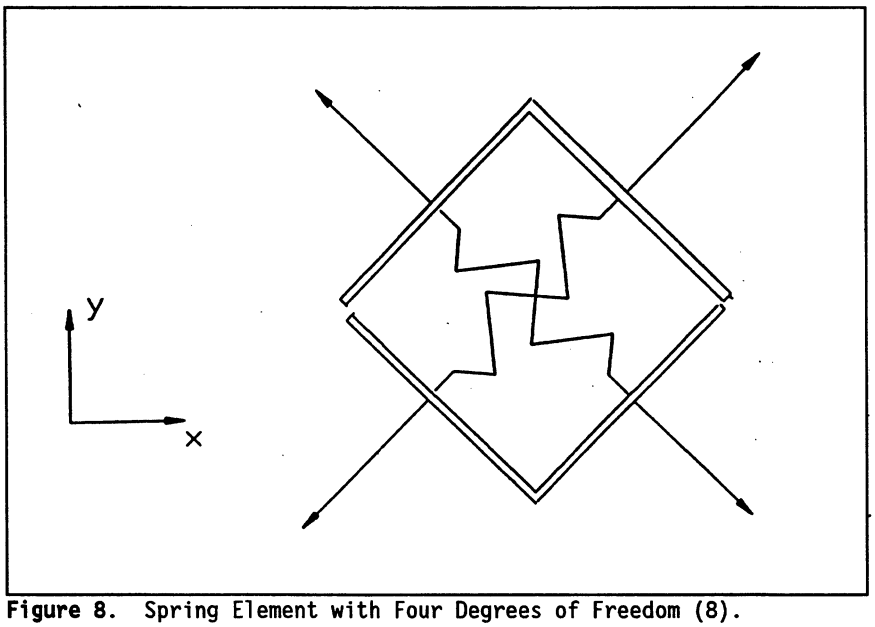


Figure 8. Spring Element with Four Degrees of Freedom (8).

Creep Model

Creep is defined as time dependent deformation of a material subjected to sustained stress or loading. In the case where deformation is kept constant due to some restraint, creep reduces stress in concrete, which is known as relaxation. Creep due to thermal and shrinkage strains is included in this analysis. The method of superimposition of virgin creep curves is applied in this analysis and is similar to the approach by Grzybowski (6). At any time t, the creep

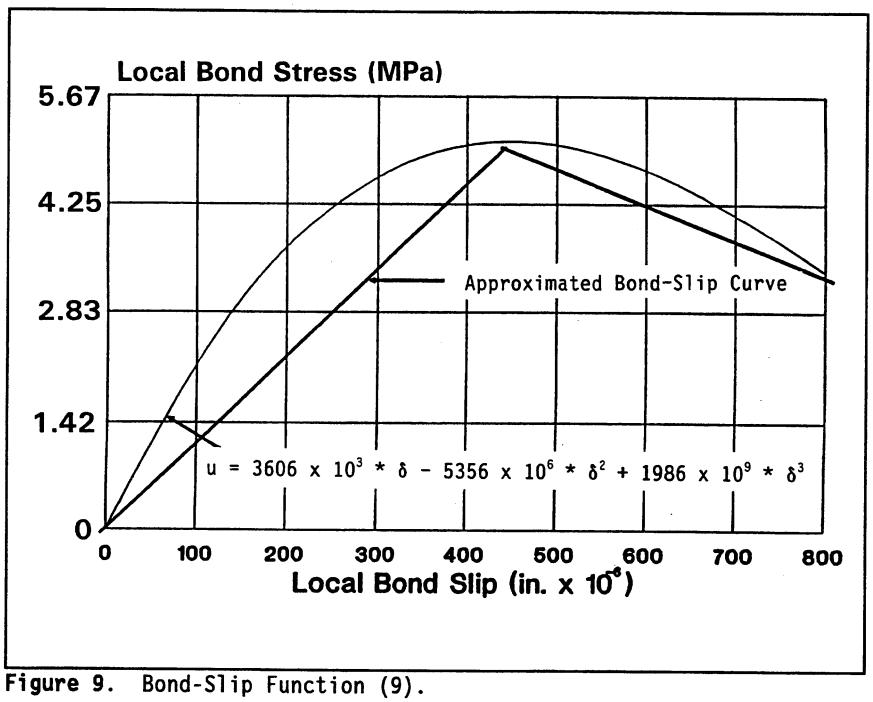


Figure 9. Bond-Slip Function (9).

function used to determine creep due to a load increment applied at time t_o is given by:

$$\Phi(t,t_o) = \frac{1}{E(t_o)}[1+\phi(t,t_o)] \quad [12]$$

where

- $E(t_o)$ = elastic modulus at age t_o (MPa)
- $\phi(t, t_o)$ = creep coefficient (ACI code)
- t = actual age of concrete (days)
- t_o = age of concrete at which load was applied (days)

For every increment of stress $\Delta\sigma_i$, the strain increment in the 'i'th time step due to creep effect is given by the following equation:

$$\Delta\epsilon_i = \frac{\Delta\sigma_i}{E(t_o)}[1+\phi(t,t_o)] \quad [13]$$

The coefficient of creep in this analysis is suggested by the American Concrete Institute (11) as a function of time and material properties. It is defined by the following equation:

$$\phi(t,t_o) = \frac{(t-t_o)^{0.6}}{10+(t-t_o)^{0.6}}\,\phi\infty(t_o) \quad [14]$$

where

- t = time at which creep coefficient is computed
- t_o = time at which load is applied
- $\phi\infty$ = ultimate creep coefficient, as given in ACI, depends on type of mix, specimen geometry, relative humidity, and age of concrete.

The ultimate creep coefficient is defined as the ratio of creep strain to initial strain. Its range, as specified in ACI, is normally between 1.30 and 4.15. The average value of the ultimate creep coefficient for moist cured concrete is given by:

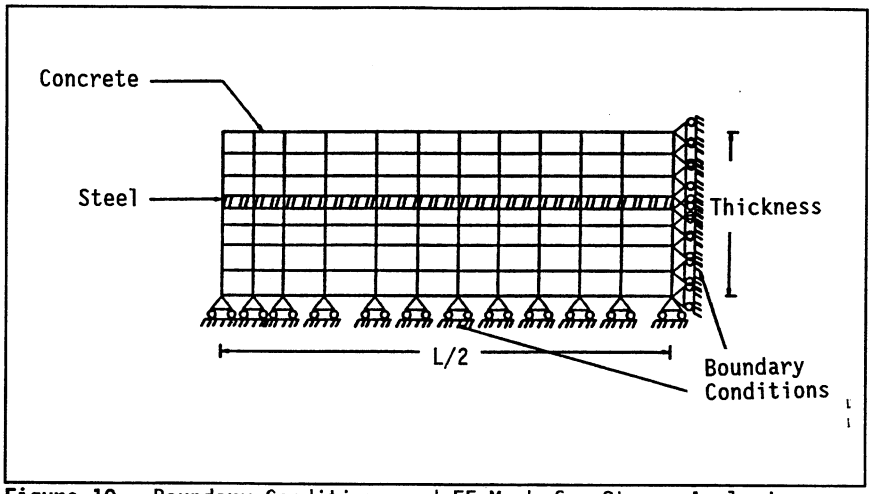


Figure 10. Boundary Conditions and FE Mesh for Stress Analysis.

$$\phi_\infty = 2.35\gamma_c \quad [15]$$

where γ_c is the correction factor, which depends on the relative humidity. This is given as:

$$\gamma_c = 1.27 - 0.067h \quad [16]$$

where h is the moisture content in concrete. Creep is defined as time dependent deformation of a material subjected to sustained stress or loading.

EXAMPLE ANALYSIS

Four example problems are considered to study various features of the model developed for the study of shrinkage and temperature stresses in CRC pavements. The finite element mesh for the stress analysis model is optimally refined by considering mesh models with different aspect ratios.

The performance of the stress analysis model and its results are compared with Vetter's theoretical model (1). An example problem of uniform shrinkage is considered for the analysis to verify the model. The various parameters required for the analysis (both for the developed model and Vetter's model) are given below:

Crack spacing (L) = 2.5 m

Concrete Poisson ratio = 0.18

Steel Poisson ratio = 0.3

Concrete Elastic modulus (E_c)= 30,000 MPa

Steel Elastic modulus (E^s) = 206,000 MPa

Percentage area of steel (p) = 0.75%

Reinforcing bar diameter (d_b)= 19.5 mm

Reinforcement cover = 10.0 mm

Thickness of concrete slab = 25.4 cm

The following reduced equation of Vetter (1) is used for the computation of concrete stress in the pavement that occurs halfway between the transverse cracks due to drying shrinkage only:

$$f_t = \frac{-(Q') + \sqrt{(Q')^2 + 4(Q')(zE_s)}}{2} \quad [17]$$

where

f_t = average tensile stress in concrete in the middle of the slab

Q' = $L \cdot Q \cdot n \cdot p \cdot u$
Q = $4p/d_b$
p = percentage reinforcement
d_b = diameter of the reinforcing bar (mm)
n = E_s/E_c
E_s = modulus of elasticity of steel (MPa)
E_c = modulus of elasticity of concrete (MPa)
u = average bond stress (MPa)
z = shrinkage strain
L = crack spacing (m)

In the first example, the tensile stress in concrete is computed using equation 17 and compared to the tensile stress computed using the finite element analysis. The results indicated for low shrinkage strains, the maximum tensile stress in the concrete, as computed by the FE model, is near the location of the steel reinforcement. However, note in Figure 11, that the location of the maximum bond stress becomes further away from the crack face as the shrinkage strains increase. This may be primarily due to the varying level of restraint of the steel reinforcement near the crack face and the nature of the bond-slip function. The significance of this is that the maximum tensile stress also occurs further away from the crack face with an increase in shrinkage strains. As the shrinkage increases, a greater breakdown of the bond near the crack face occurs which reduces the concrete tensile stress in the vincity of the bond breakdown. This leads to the maximum stress occurring at and moving with the fully bonded region as illustrated in Figures 12 and 13 under a shrinkage strain of 100 ms.

To compare the results with Vetter's equation (1), the average concrete stress (average of all stresses along the section at which maximum bond stress occurs) is determined from the FE analysis and plotted in Figure 12. It is observed that even though the maximum concrete stress obtained from the numerical model is high, the average stress is nearly equal to values obtained from Vetter's equations. As pointed out above, the bond stress distribution as computed from the FE model for various shrinkage strains are as shown in Figure 11. The Vetter approach assume the bond to be uniformly distributed over the length of the bond development. In this sense, the FE model represents the bond distribution in a more realistic manner than does the Vetter equation. Stress contours for a shrinkage of 100 microstrain (ms), uniformly distributed along the depth are illustrated in Figure 13 and the slab boundary conditions are as shown in Figure 10. This figure indicates, as pointed out previously, that the maximum stress occurs near the steel reinforcement in the vicinity of the fully bonded region. This point is further illustrated in Figure 14, which shows the maximum concrete stress distribution along the reinforcement for the analysis shown in Figure 13.

The second example considers a non-uniform, vertical shrinkage and temperature distribution and is presented to further illustrate the model capabilities in terms of concrete cover over the steel reinforcement, bond stress-slip effects, and the percentage of steel reinforcement. It is pointed out that the Vetter approach does not consider the effect of either rebar cover or

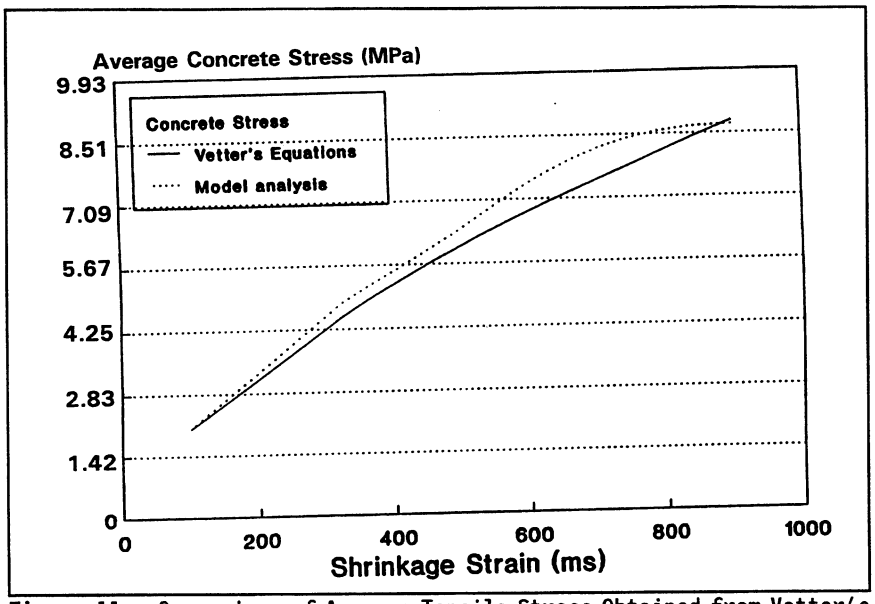


Figure 11 Comparison of Average Tensile Stress Obtained from Vetter's Equations and Stresses Model.

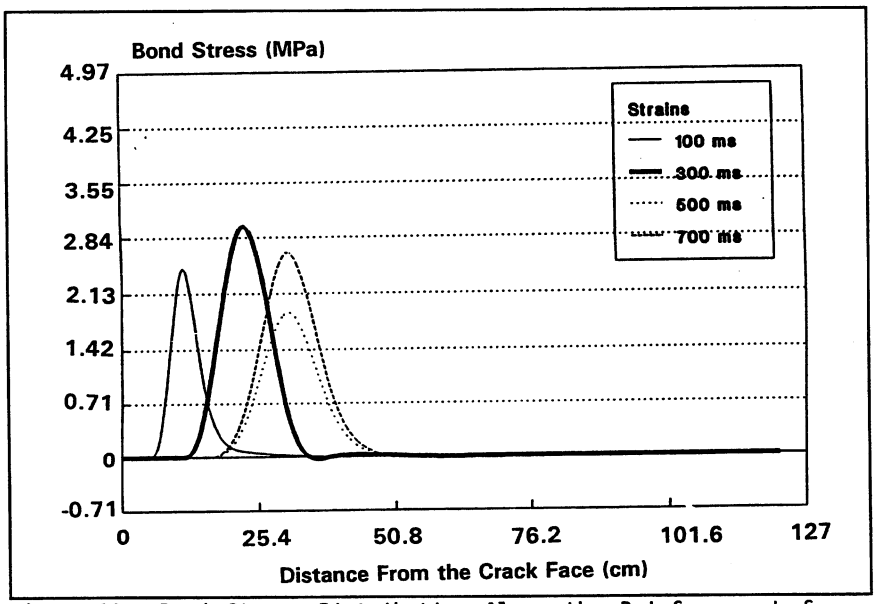


Figure 12. Bond Stress Distribution Along the Reinforcement for Different Uniform Shrinkage Strains.

non-uniform shrinkage or temperature gradients. The shrinkage strain is allowed to vary through the depth of the concrete and nonlinear moisture diffusivity is considered in the analysis.

It is observed that the diffusivity constant in equation 5 of the diffusion theory is nonlinear with respect to time. The variation of diffusivity, which is obtained from experimental data, is provided in the literature (19). The following regression equation is developed from the data (equation 17):

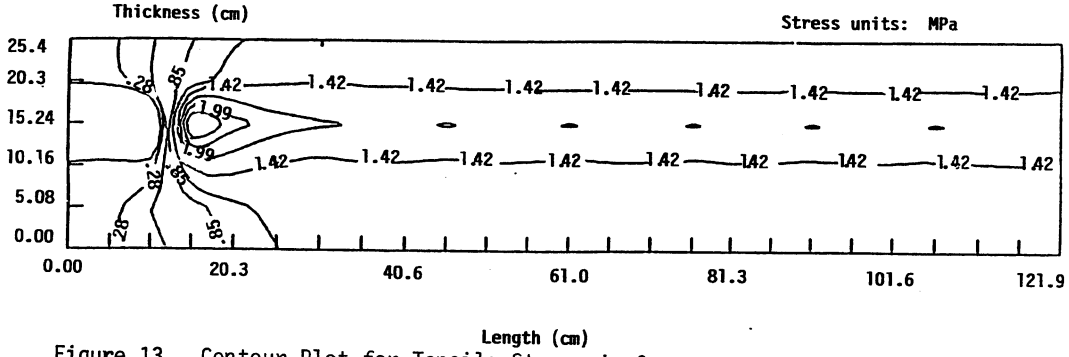


Figure 13. Contour Plot for Tensile Stress in Concrete for 100 ms Uniform Shrinkage Strain.

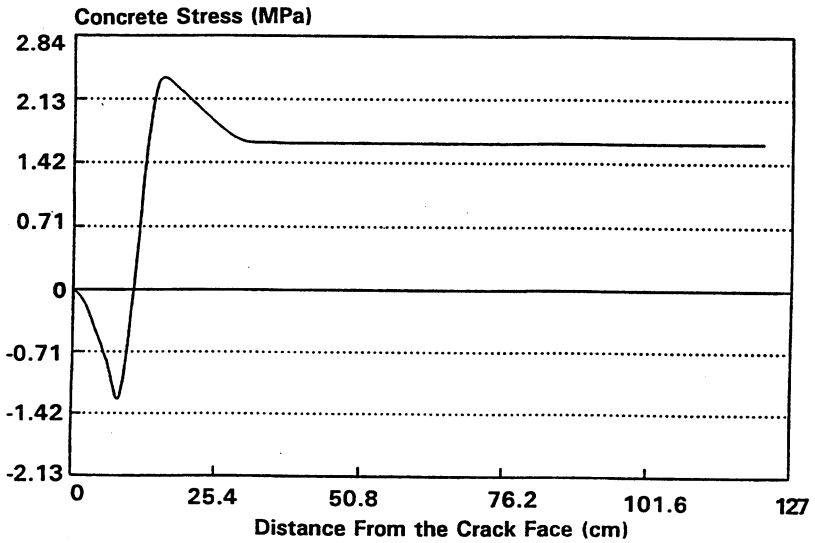


Figure 14. Concrete Stress Distribution Along the Reinforcement for 100 ms Uniform Shrinkage Strain.

$$k_h=(-0.000078e^{t}+2.3614626e^{-t}+0.2486424)(2.54)^2$$

where

k_h = diffusivity (cm^2/day)
t = time (day)

A pavement with a thickness of 10 inches is assumed to illustrate the effects of the above factors in which ambient conditions are idealized. The variation of the ambient temperature and relative humidity for the pavement construction site conditions are approximated by a sine curve. The maximum temperature is assumed to be 90 degrees Fahrenheit, and the minimum temperature at midnight is assumed to be 60 degrees Fahrenheit. A 30-degree Fahrenheit variation over a twenty-

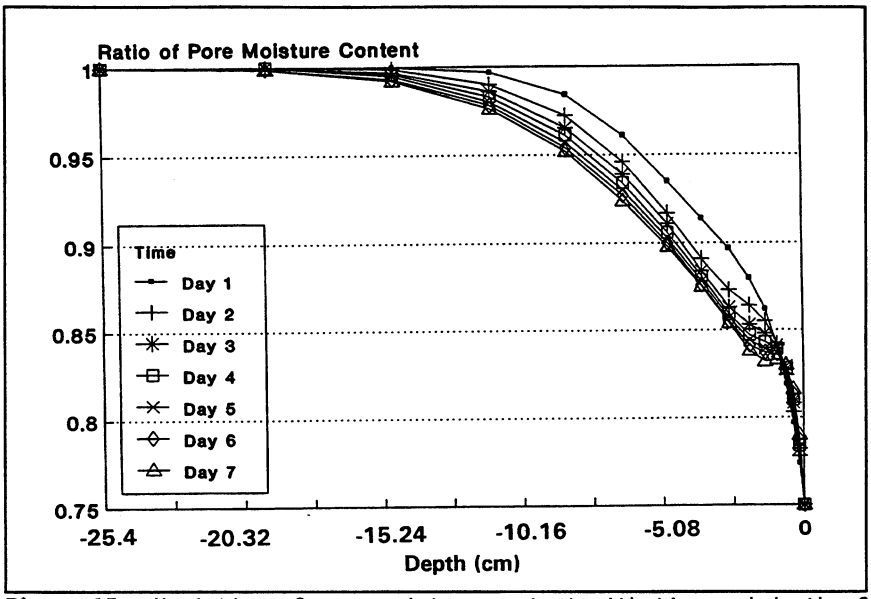


Figure 15. Variation of pore moisture content with time and depth of pavement.

four hour period is assumed. Similarly, the maximum relative humidity is assumed to be 90%, and the minimum relative humidity is taken to be 60%, with a variation of 30% relative humidityover a 24 hour period. Analysis begins with themean temperature and relative humidity. The sine curves of the relative humidity and temperature are shifted by a phase angle of 180 degrees; i.e., the maximum temperature andminimum relative humidity are observed at noon and maximum relative humidity and minimum temperature are observed at midnight. The variation of temperature along the depth of the concrete is taken into consideration with a gradient of +0.8 degrees and -0.4 degree per centimeter for the day and night (maximum and minimum) temperatures, respectively. A thermal coefficient of 5 micro strains per degree Fahrenheit was assumed for the concrete and 6 micro strains per degree Fahrenheit for the steel reinforcement.

The results (Figure 15) show that the rate of diffusion of the moisture decreases with time. This is expected because the diffusivity constant decreases with time. It is also observed that even though the net ambient conditions are constant, there is a Shrinkage strains are computed from the pore moisture content using equation 6. The maximum diffusion of moisture from the pavement is observed at noon due to high temperature and low relative humidity. These shrinkage strains and temperature differentials are used as the input for three cases that are analyzed to study the effect of the reinforcement cover on the stress distribution in CRC pavements. These cases are as follows:

a) The steel reinforcement at a depth of 5 cm

b) The steel reinforcement at a depth of 10 cm

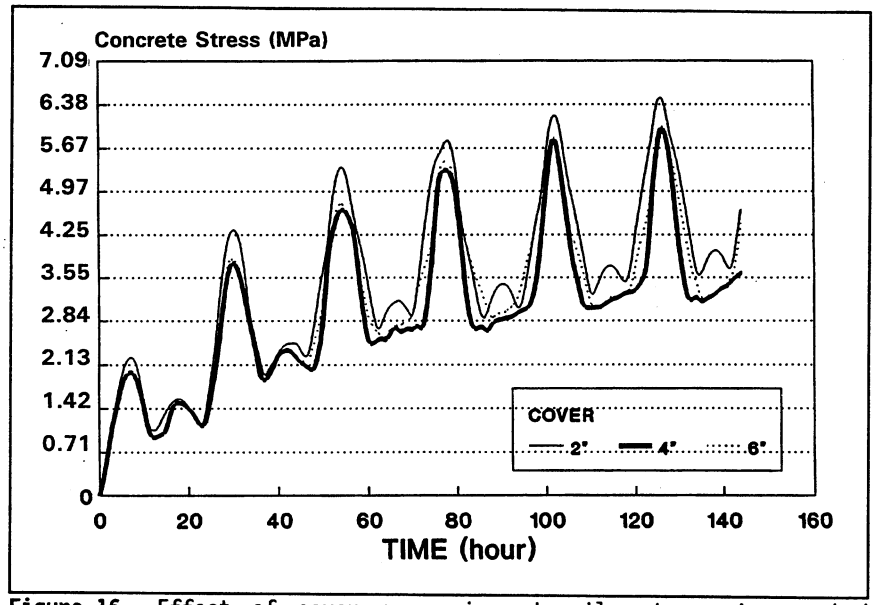


Figure 16. Effect of cover on maximum tensile stress in cracked pavement.

c) The steel reinforcement at a depth of 15 cm

Values for shrinkage strain and temperature differentials are taken from the strain model.

In the above analysis, it is observed that the location of the maximum concrete tensile stresses occur again at the level of the steel. This may be contrary to the commonly held belief that the maximum stresses occur near the pavement surface. Also, the maximum stress location is apparently at the point where the concrete is perfectly bonded to the reinforcement and the bond slip is nil. The effect that rebar cover is illustrated in the Figure 16. It is observed from the analysis, that a 5 centimeter cover of the slab steel produces greater tensile stress in concrete when compared to 11.2 centimeter of cover. Field observations (12) have indicated that CRC pavements with shallow rebar covers tend to develop, on the average, closer crack patterns than those with greater depths of cover. In the perception that greater stresses result in a higher degree of cracking, past field studies tend to verify this result. It is pointed out this effect was not observed under a uniform shrinkage distribution since the strain field was linearly distributed. As the steel is positioned nearer the high temperature and moisture gradient area, an increase in the concrete stresses result due to the bonding between steel and concrete increasing the level of restraint.

The third example demonstrates the effect of varying the percentage of steel reinforcement on the maximum tensile stresses and the effect of the percentage of steel on stress

distribution in the pavement. Two cases are analyzed:

a) 2 inches cover with 0.75% steel reinforcement.

b) 2 inches cover with 0.50% steel reinforcement.

The variation of the steel reinforcement is represented by varying the thickness of the reinforcement and the diameter of the reinforcing bar. Figure 17 illustrates the maximum tensile stress in concrete for these two cases. The variation of maximum tensile stress due to the variation of the percentage of steel is not significant, even though stresses in the case of 0.75% steel are lesser than stresses in concrete with 0.50% steel, which is not consistent with other analytical models.

The final example considers the effect of the bond stress-slip relationship. In the field, it is observed that the bond between steel and concrete varies significantly between epoxy-coated bars and ordinary deformed bars. An approximate variation of the stiffness of the bond slip elements is considered to show the effect of bond on stress distribution. Figure 18 illustrates the two bond slip relationships considered for this analysis. The slope of the bond stress-slip for low stiffnesss curve (Figure 18) is 50% of that for high stiffness curve. The analysis is performed for a cover of 5 centimeters and the results are illustrated in Figure 19. It is observed that in the first few hours there is no difference in the stress between the two above-mentioned cases; however after 60 hours, the stresses in lower bond strength increase significantly. This can be explained by the fact that the bond between steel and concrete fails (low stiffness curve) and hence gives higher tensile stress in concrete due to the fact that all the stresses are carried by the concrete only. Also, tensile stresses in the concrete are high in both cases due to the presence of steel in the high strain gradient area.

The above four example problems describe the potential capabilities of the analysis framework. Also the effect of the ambient temperature and ambient humidity on the CRC pavements is illustrated for various reinforcement covers and bond slip relationships.

CONCLUSIONS AND RECOMMENDATIONS

A procedure for a numerical analysis framework is developed to determine shrinkage strains and the corresponding tensile stresses in reinforced concrete slabs. Even though previous literature addresses these problems, most models either do not consider the nonuniform distribution of shrinkage strains or the bond slip variation in the concrete. In this paper, a framework is developed that considers not only these effects, but how they vary with respect to ambient climatic conditions in addition to creep relaxation.

Consideration of the effect of the various parameters, and the effect of their nonlinearity

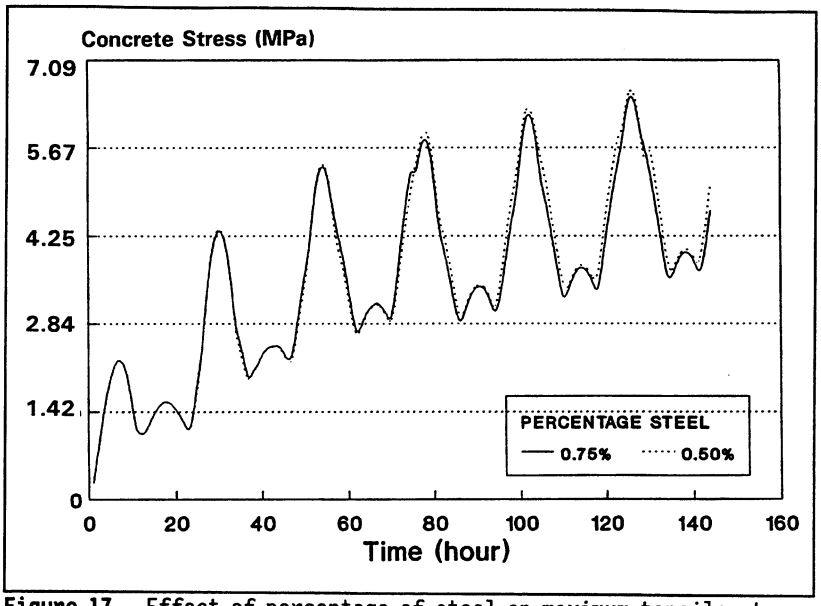


Figure 17. Effect of percentage of steel on maximum tensile stress in cracked pavement.

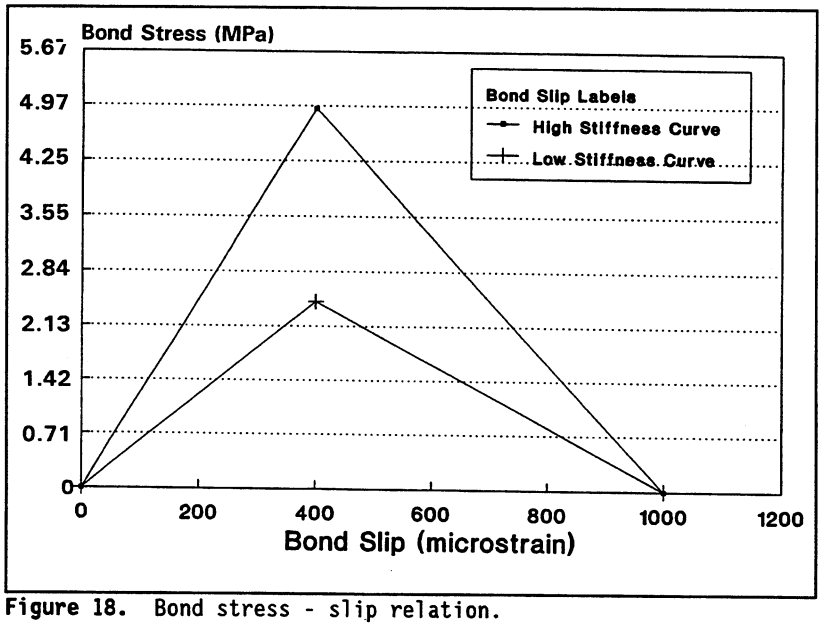


Figure 18. Bond stress - slip relation.

with respect to time, is critical to understand the pavement behavior in first few days of its construction. The frame work developed in this research, incorporates various factors that are ignored in previous pavement models. This, relatively speaking, a step beyond previous research efforts to characterize stresses in CRC pavement.

The following are the conclusions resulting from the analysis of the example cases:

a) Vetter's equations or the later modified models may be applied for predicting the average tensile stress in the middle of crack

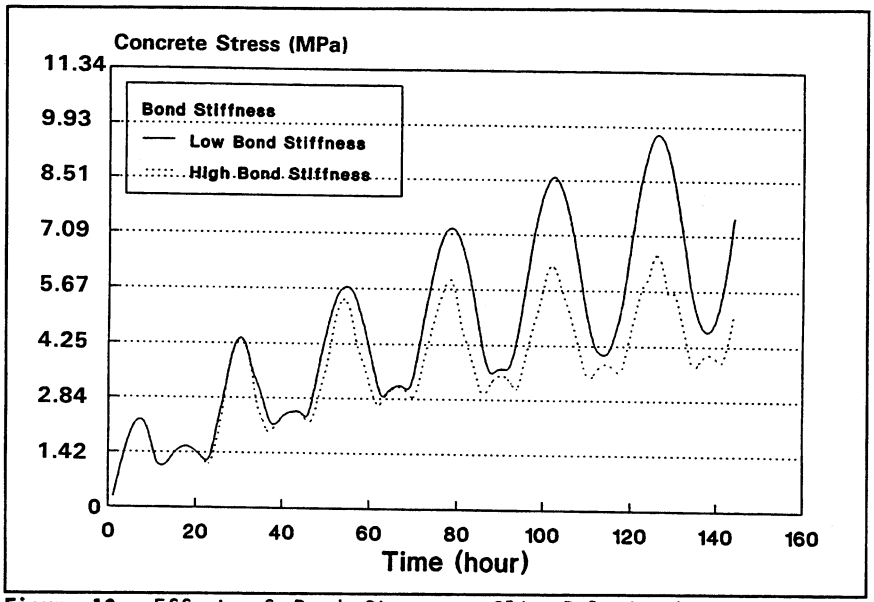


Figure 19. Effect of Bond Stress - Slip Relationship on Maximum Tensile Stress in Cracked Concrete Pavement.

spacing; however, it is observed that due to the bond between steel and concrete, maximum tensile stress in concrete is observed at the level of steel for pavements with 5 centimeters of cover, and in the middle of crack spacing for pavements with 15 centimeters of cover. Also, the maximum tensile stress predicted in this paper is greater than the average tensile stress predicted by Vetter's equations. Hence, for detailed stress analysis in the prediction of cracking, the assumption of uniform shrinkage and temperature gradients as considered in Vetter's approach may not be applicable.

b) The reinforcement cover may become a significant factor in crack development, especially under field conditions where the variation of temperature throughout a day is greater than what is assumed in this study (30° Fahrenheit over a 24-hour period).

c) More detailed research should be performed toward determination of the bond-slip relationship between the steel reinforcement and the rebar because of its apparent significant effect on stress distribution in concrete. Further research needs to be performed to more accurately determine the bond stress-slip relationship. Determination of bond characteristics between steel and concrete for different types of steel bars, such as plain, deformed, or epoxy-coated bars is significant for the prediction of the actual state of stress in CRC pavement. Although there are some experimental relationships that predict bond stress for a given slip, they are mostly pull-out types of experiments (steel bar embedded in concrete being pulled out and then studied for the strains developed in the bar and concrete). The validity of these models for the problems considered here should be studied further. Also, the model should be improved to consider

different stiffnesses for spring elements along the reinforcement since it is demonstrated that the bond stress-slip relationship varies along the reinforcement. The variation of bond stress-slip relationship with time should also be determined. The simplified assumption that this variation is proportional to the variation of the modulus of concrete was used in this paper. There is no available evidence in the literature to substantiate this assumption.

d) The analysis indicates a lack of sensitivity to the percentage of reinforcement on concrete stress. This may have been due to the FE representation used for the steel bar. It is recommended that further analysis of this effect be considered, perhaps using a different technique to represent the steel bar.

e) The model results should be verified with experimental results, which was beyond the scope of this particular study. Work is currently underway at Texas A&M University to obtain sufficient field data to valid analysis of the nature presented in this framework.

f) The model is limited to the prediction of maximum tensile stress. Hence, for a study of the actual crack mechanism and its propagation, a crack tip element should be included in the model. This will allow the model to provide a more realistic approximation of the field conditions.

g) The inclusion of all the ambient factors such as concrete creep model, temperature, and nonlinearity of the diffusion model in the analysis leads to a better understanding of the behavior of the pavement and can aid in development of a reliable design procedure for CRC pavements.

REFERENCES

1. C. P. Vetter. "Stresses in Reinforced Concrete Due to Volume Changes." *ASCE proceedings*, Paper No. 1848, Feb 1932.

2. B. F. Friberg. " Frictional resistance under Concrete and Restraint Stresses in Long Reinforced Slabs." Highway Research Board Proceedings. Vol. 33, Page 167-184, 1954.

3. Mooncheol Won, Kenneth Hankins and B. Frank McCullough. "Mechanistic Analysis of Continuously Reinforced Concrete Pavements Considering Material Characteristics, Variability and Fatigue." Center of Transportation Research, University of Texas at Austin, 1990.

4. Z. P. Bazant and L. J. Najjar. "Drying of Concrete as a Nonlinear Diffusion Problem." *Cement and Concrete Research*, Vol. 1, 1973, p 461-73.

5. N. J. Gardner and S. M. Poon. "Time and Temperature Effects on Tensile, Bond, and Compressive Strengths." Title No. 73-31, *ACI Journal*, July 1976.

6. M. Grzybowski and S. P. Shah. "Model to Predict Cracking in Fibre Reinforced Concrete Due to Restrained Shrinkage". *Magazine of Concrete Research*, 41, No. 148, Sep. 1989, p. 125-135.

7. Royall D. Bradbury. *Reinforced Concrete Pavements*. Wire Reinforcement Institute, Washington, D. C., 1938.

8. D. Ngo and A. C. Scordelis. "Finite Element Analysis of Reinforced Concrete Beams." Title No. 64-14, *ACI Journal*, March 1967.

9. A. H. Nilson. "Nonlinear Analysis of Reinforced Concrete by the Finite Element." *ACI Journal*, Title No. 65-55, Sep. 1968.

10. J. W. Wesevich, B. F. McCullough and N. H. Burns "Stabilized Subbase Friction Study for Concrete Pavements." Research report 459-1. Center of Transportation Research, University of Texas at Austin, 1990.

11. ACI Manual of Concrete Practice - 1990 Vol I-IV. *American Concrete Institute*, 1990.

12. Dan G. Zollinger and Ernest J. Barenberg. "Continuously Reinforced Pavements: Punchouts and Other Distresses and Implications for Design." Project IHR - 518, Illinois Cooperative Highway Research Program, University of Illinois, Urbana, Illinois, March, 1990.

13. Arthur H. Nilson. "Bond Stress-Slip Relations in Reinforced Concrete". Report No. 345, Department of Structural Engineering, School of Civil and Environmental Engineering, December 1971.

14. R.P. Palmer, M. Olsen, and R.L. Lytton, "TTI CRCP - A Mechanistic Model for the Prediction of Stresses, Strains, and Displacements in Continuously Reinforced Concrete Pavements," Research Report 371-2F, Texas Transportation Institute, Texas A&M University, August 1987, 275pp.

15. D.E. Branson, *Deformation of Concrete Structures*. McGraw-Hill, New York, 1977.

16. Tianxi Tang, Dan G. Zollinger, and B. Frank McCullough, "LaPorte Test Sections," Technical Memorandum, Texas DOT, November 9, 1992.

17. M. Grzybowski, "Determinaiton of Crack Arresting Properties of Fiber Reinforced Cementitious Composites," Publication TRITA - BRO - 8908, Department of Structural Engineering, Royal Institute of Technology, Stockholm, Sweden.

18. Z.P. Bazant and S.T. Wu, "Creep and Shrinkage Law for Concrete at Variable Humidity," *Journal of the Engineering Mechanics Division*, Vol. 100, Dec., 1974.

19. Zdenek P. Bazant and L. Panula, "Practical Prediction of Time - Dependent Deformations of Concrete. Part I: Shrinkage. Part 2: Creep," *Materiaux et Constructions*, Vol. 11, No. 65, Sept.-Oct. 1978, pp. 307-328.

20. D.H. Jiang, S.P. Shah, and A.T. Andonian, "Study of the Transfer of Tensile Forces by Bond," *ACI Journal*, Proceeding, Vol. 78, No.3, May-June 1981, pp. 217-225.

21. Mooncheol Won, B Frank McCullough, and W.R. Hudson, "Evaluation of Proposed Texas SDHPT Design Standards for CRCP," Research Report 472-1, Center for Transportation Research, The University of Texas at Austin, April 1988.

22. A.M. Ioannides, M.R. Thompson, and E.J. Barenberg, "Westergaard Solutions Reconsidered," *Transportation Research Record 1043*, Transportation Tesearch Board, National Research Council, Washington, D.C., 1985, pp. 13-23.